

1 **Characterization of HAZ of API X70 Microalloyed Steel Welded by Cold-wire Tandem** 2 **Submerged Arc Welding**

3 MOHSEN MOHAMMADIJOO¹, STEPHEN KENNY^{1,2}, LAURIE COLLINS², HANI HENEIN¹, and DOUGLAS
4 G. IVEY^{1,*}

5 ¹Department of Chemical and Materials Engineering, University of Alberta, Edmonton, AB, Canada T6G 1H9

6 ²R&D Division, Evraz Inc. NA, P.O. Box 1670, Regina, SK, Canada S4P 3C7

7 *Corresponding author. Prof., Ph.D.; Tel.: +1 780 4922957; Fax: +1 780 4922881

8 E-mail address: divey@ualberta.ca (D.G. IVEY)

9 **ABSTRACT**

10 High strength low carbon microalloyed steels may be adversely affected by the high heat input and thermal cycle
11 that they experience during tandem submerged arc welding (TSAW). The heat affected zone (HAZ), particularly the
12 coarse grained heat affected zone (CGHAZ), i.e., the region adjacent to the fusion line, has been known to show
13 lower fracture toughness compared with the rest of the steel. The deterioration in toughness of the CGHAZ is
14 attributed to the formation of martensite-austenite (M-A) constituents, local brittle zones (LBZ) and large prior
15 austenite grains (PAG). In the present work, the influence of the addition of a cold wire at various wire feed rates in
16 cold-wire tandem submerged arc welding (CWTSAW), a recently developed welding process for pipeline
17 manufacturing, on the microstructure and mechanical properties of the HAZ of a microalloyed steel has been
18 studied. The cold wire moderates the heat input of welding by consuming the heat of the trail electrode.
19 Macrostructural analysis showed a decrease in the CGHAZ size by addition of a cold wire. Microstructural
20 evaluation, using both tint etching optical microscopy (TEOM) and scanning electron microscopy (SEM), indicated
21 the formation of finer PAGs and less fraction of M-A constituents with refined morphology within the CGHAZ
22 when the cold wire was fed at 25.4 cm/min. This resulted in an improvement in the HAZ impact fracture toughness.
23 These improvements are attributed to lower actual heat introduced to the weldment and lower peak temperature in
24 the CGHAZ by cold wire addition. However, a faster feed rate of the cold wire at 76.2 cm/min adversely affected
25 the toughness due to the formation of slender M-A constituents caused by the relatively faster cooling rate in the
26 CGHAZ.

27 **Keywords:** Martensite-austenite constituent, Toughness, Microhardness, Welding process, Microalloyed steel.

28 **I. INTRODUCTION**

29 Tandem submerged arc welding (TSAW), i.e., submerged arc welding with two to five electrodes [1–3], has
30 been extensively utilized to fabricate high strength low alloy steel pipelines, pressure vessels, structures and wind
31 turbine towers [4,5]. TSAW offers several advantages over other welding processes, such as high deposition rate,
32 deep penetration, high quality welds and the ability to weld thick plates due to its high heat input [6,7]. The fracture
33 toughness of the heat affected zone (HAZ), particularly the coarse grained heat affected zone (CGHAZ), of
34 microalloyed steel welds tends to weaken due to the high heat input and thermal cycles that the steel experiences
35 during welding. The reduction in toughness in the CGHAZ is attributed to the formation of large prior austenite
36 grains (PAGs) and martensite-austenite (M-A) constituents, which are characterized as localized brittle zones (LBZ),
37 as a result of the high peak temperature and relatively fast cooling rate in the CGHAZ [8–12]. Davis et al. [13,14]
38 and Reichert et al. [15] found that the formation of a network of enlarged M-A constituents along the PAG
39 boundaries resulted in cleavage crack initiation in the HAZ. Moeinifar et al. [16] suggested that a reduced fraction
40 of M-A constituents in the CGHAZ was beneficial to the impact toughness. However, the fraction and size of M-A
41 constituents are essentially dependent on the PAG size. Yu et al. [10] and Li et al. [11] showed that the fraction and
42 shape of M-A constituents were increased by coarsening the PAG size in the CGHAZ. They found that a coarse
43 PAG size, associated with coarse M-A constituents, is the dominant factor in promoting brittle fracture in the
44 CGHAZ. Gharibshahian et al. [17] reported that the formation of coarser PAGs in the CGHAZ has a detrimental

45 effect on the toughness of the HAZ. Yang and Bhadeshia [18] and Garcia-Junceda et al. [19] showed that the
46 martensite start temperature (Ms) increases with an increase in the PAG size, which results in a higher volume
47 fraction of martensite.

48 In the present work, cold-wire TSAW (CWTSAW) is developed to improve the microstructure and the
49 mechanical properties of the HAZ of a X70 microalloyed steel weld, while retaining appropriate weld geometry.
50 The additional cold wire fed into the tandem weld pool essentially increases the deposition rate, resulting in better
51 welding productivity for the welding process without increasing the heat input compared with the TSAW
52 process [20–22]. In our previous studies [23,24] the CWTSAW process parameters were correlated with the
53 dilution, geometry characteristics and microhardness properties of the weld metal (WM) and HAZ. Incorporating a
54 cold wire in TSAW moderates the heat input through transfer of some of the excess energy of the trail electrode,
55 which lowers the amount of heat introduced to the weldment [20–22]. Accordingly, better quality welds were
56 achieved at lower heat inputs per mass of deposited material and with a substantial reduction in arcing time leading
57 to the formation of a smaller and shorter weld pool (compared with TSAW without a cold wire) [23,24]. As such,
58 CWTSAW technology is a promising technique for pipe seam welds commonly used in the pipeline industry. The
59 present study characterizes the macrostructure, mechanical properties and microstructure alterations in the HAZ of a
60 typical microalloyed steel and their evolution by varying the cold wire feeding rate in the CWTSAW process.
61 Microstructural characterization is carried out using tint etching optical microscopy (TEOM) and scanning electron
62 microscopy (SEM). Charpy V-notch impact testing and microhardness testing are performed to investigate and
63 correlate the properties changes with microstructure alterations in the HAZ of samples prepared by CWTSAW. The
64 geometry characteristics are analyzed using stereomicroscopy.

65 II. MATERIALS AND EXPERIMENTAL PROCEDURE

66 A. Materials and Welding Process

67 API X70 microalloyed steel plates with a thickness of 13.4 ± 0.3 mm, produced by Evraz Inc. NA through
68 thermo-mechanical controlled processing (TMCP) [25], were V-shape beveled with an angle and depth of $80^\circ \pm 5^\circ$
69 and 4 mm, respectively, prior to welding. Six welding runs at three different cold wire feed rates were carried out to
70 prepare the weld samples. The weld samples were prepared using two 4 mm diameter EA2 electrodes (according to
71 AWS-A5.23/ASME-SFA5.23) and one cold wire with the same diameter and composition as the electrodes. BF6.5
72 flux was chosen according to EN 760 (Bavaria, Germany). The chemical compositions of the microalloyed steel and
73 consumable electrodes are given in Table I. According to Easterling [26], the welding crack susceptibility of steels
74 is usually expressed in terms of a carbon equivalent that shows composition allowances to avoid cold cracking or
75 hydrogen cracking. For low carbon microalloyed steels, the welding crack susceptibility index, P_{cm} , is calculated
76 according to the Ito-Bessyo equation [27].

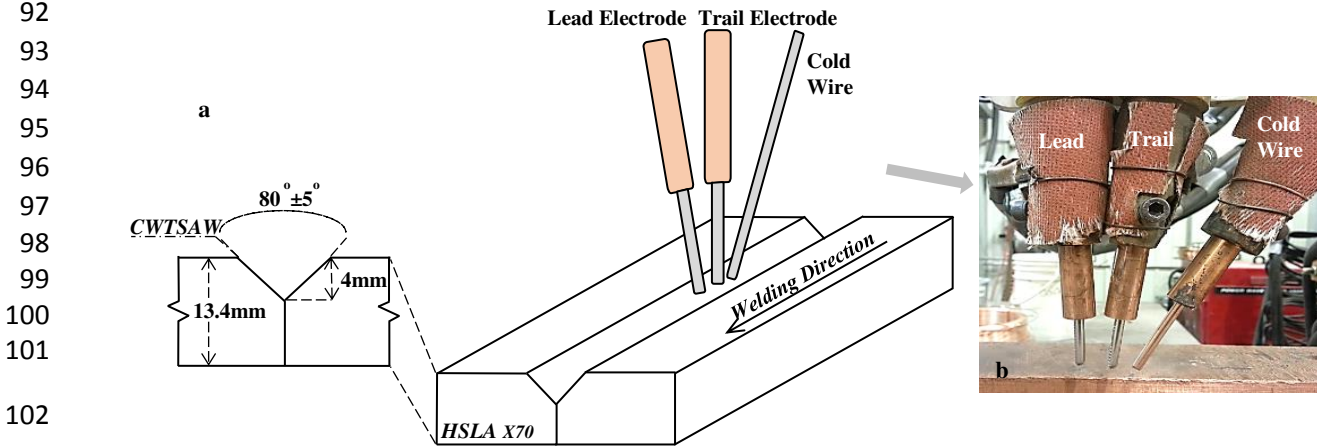
$$77 \quad P_{cm} = \%C + \frac{\%Si}{30} + \frac{\%Mn + \%Cu + \%Cr}{20} + \frac{\%Mo}{15} + \frac{\%V}{10} + \frac{\%Ni}{60} + 5\%B \quad [1]$$

78 The lead and trail electrodes were operated using direct current electrode positive (DCEP) and square wave
79 alternating current (ACSQ) polarity, respectively, with constant current type power sources. The influence of
80 CWTSAW process parameters on the geometry, dilution and microhardness of the weld and the HAZ was
81 investigated and optimized in a previous work of the authors [23,24]. The present CWTSAW process setup has
82 been developed based on the optimized welding parameters. The welding conditions to fabricate the microalloyed
83 steel joint are presented in Table II. The steel plate geometry and the CWTSAW process setup employed to fabricate
84 the weld samples are depicted in Figure 1. The heat input of the welding processes was calculated according to
85 equation 2 [28] and set at 22.2 kJ/cm.

$$86 \quad HI \left(\frac{kJ}{cm} \right) = \frac{60 \cdot \mu}{1000 \cdot S} \cdot [(V \cdot I)_{Lead} + (V \cdot I)_{Trail}] \quad [2]$$

87 where μ is the arc efficiency, which depends on the welding process, and HI , V , I and TS are the heat input, voltage,
 88 current and travel speed (cm/s), respectively. The arc efficiency for submerged arc welding is 0.9-1.0.

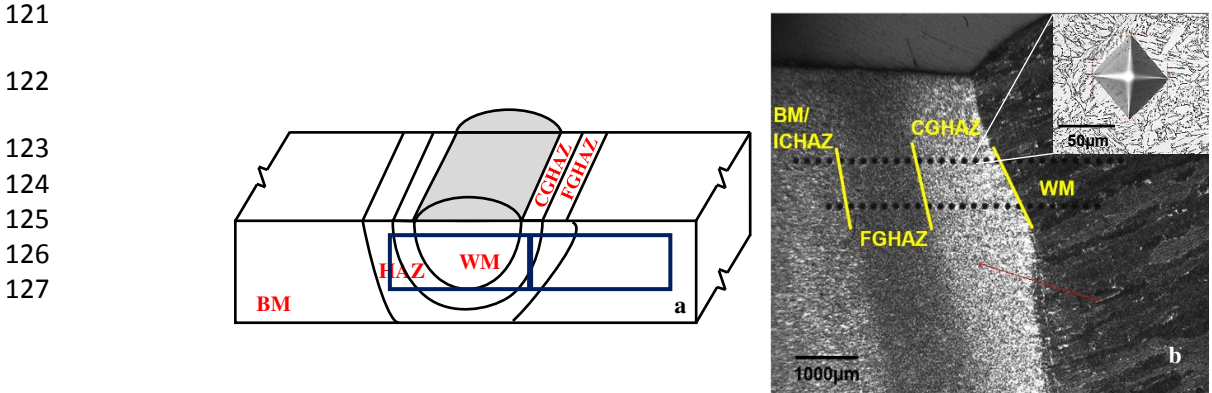
89 The weld samples were prepared by CWTSAW at cold wire feed rates of 25.4 cm/min and 76.2 cm/min and by
 90 TSAW (no cold wire), which are henceforth referred to as CW1, CW3 and TS, respectively. All welding parameters
 91 were the same for the processes other than the additional cold wire.



103 Fig. 1- CWTSAW process setup. (a) Schematic view of joint configuration along with the positioning of the
 104 electrodes and cold wire and (b) welding setup designed at Evraz Inc. NA.

105
 106 **B. Microstructure and Mechanical Testing**

107 Due to the bulbous shape of the weld metal and the HAZ and the relatively small size of the HAZ, it was not
 108 possible to fabricate full size Charpy specimens of the HAZ. As such, subsize Charpy V-notch (CVN) specimens (5
 109 mm x 10 mm x 55 mm) were machined along the transverse welding direction according to ASTM E23-12c [29].
 110 These were extracted as close to the top metal surface as possible to ensure that half of the notch was located in the
 111 CGHAZ and half was located in the fine grained heat affected zone (FGHAZ). In order to position the V notch in the
 112 HAZ, the specimens were firstly macro-etched with 5% Nital to outline the HAZ boundaries. The Charpy impact
 113 tests were then performed at room temperature (RT), 243 K (-30°C) and 228 K (-45°C) and at least five specimens
 114 per weld condition and temperature were tested. Figure 2(a) illustrates the location of the notch for the toughness
 115 investigation. To analyze the microhardness variation along the weld samples (ASTM E384 [30]), two transverse
 116 samples from each weld were extracted according to ASTM E3-11 [31] to increase the number of data sets. A 500 g
 117 load was applied for a dwell time of 14 s per indentation using a Wilson-VH3300 microhardness machine (Buehler,
 118 Germany). In total, forty test points were examined per weld, with an average of 14-18 indents across each of the
 119 FGHAZ and CGHAZ. Figure 2(b) depicts the hardness measurement mapping along a weld sample fabricated using
 120 CWTSAW.



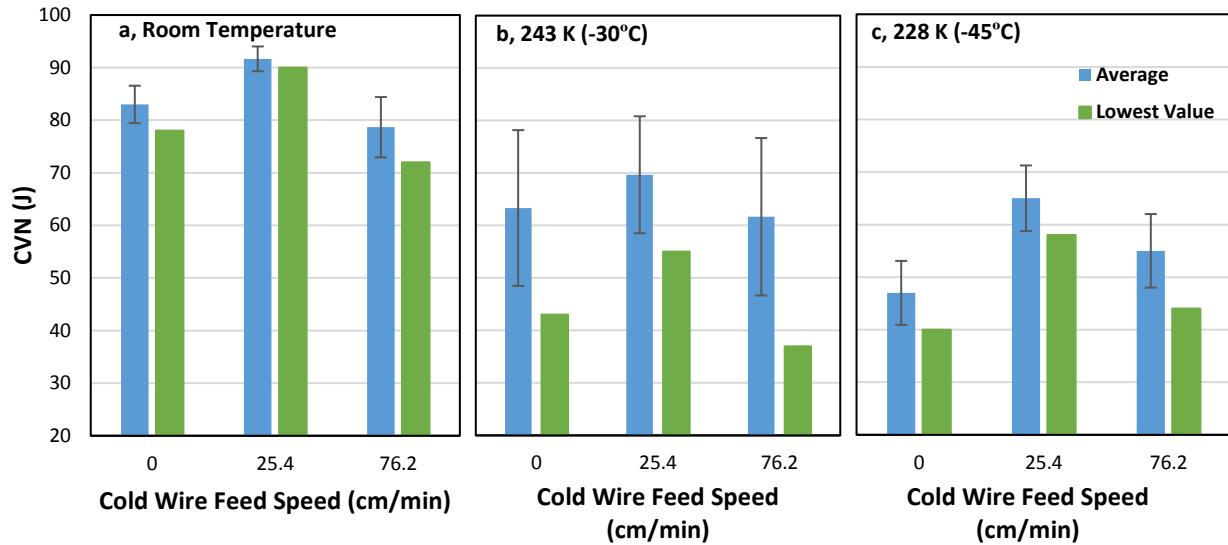
128 Fig. 2- (a) Schematic view of the CVN specimen extraction from the weld sample. (b) Microhardness mapping
129 along the BM, HAZ and WM of a typical weld prepared by CWTSAW. The micrograph in the inset shows an
130 indentation in the CGHAZ.

131
132 Optical microscopy (Olympus BX61) and scanning electron microscopy (Tescan Vega-3 SEM) were utilized to
133 analyze the microstructural changes along the HAZ. The formation and fraction of M-A constituents is dependent on
134 the cooling rate and the PAG size [11,12,32]. Revealing PAG boundaries and M-A constituents in microalloyed
135 steels and their relevant welds can be difficult to achieve and depends very much on the etchant type and time. As
136 such, several etching procedures, using various etchants with different solution concentrations and etching times,
137 were employed. After the etching trials, a chemical solution containing 4 g of picric acid in 96 ml ethanol along with
138 a few drops of HCl acid was selected to reveal the PAG boundaries. The PAG size was analyzed using the mean
139 linear intercept method according to ASTM E112 [33]. Freshly polished weld specimens were then tint etched
140 through a separate process using modified LePera's etchant [34,35] for 30-50 s to reveal different microstructural
141 features. Microstructural analysis indicated a high sensitivity for phase identification to etchant composition and
142 etching time. Quantitative analysis of the M-A constituent was done using ImageJ commercial image analysis
143 software. The fraction of other microstructure features was examined according to ASTM E562 [36]. Fracture
144 analysis of the CVN specimens was carried out by SEM.

145 III. RESULTS

146 A. Charpy Impact Toughness

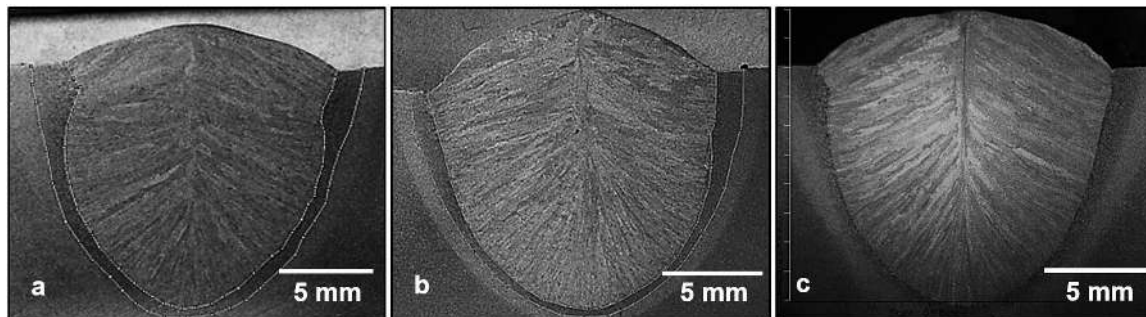
147 The average of the Charpy results and the minimum impact energy for each weld are presented in Figure 3. The
148 minimum Charpy absorbed energy represents the lowest toughness that was measured and may be important from a
149 practical perspective. According to Figure 3, the impact energy (both the average and minimum values) increased at
150 the different testing temperatures when the cold wire was fed at 25.4 cm/min compared with the conventional TSAW
151 process. However, the Charpy results showed no improvement when the cold wire was fed at 76.2 cm/min. Given
152 the fact that fracture toughness of microalloyed steels is influenced by a number of microstructural factors, such as
153 grain size, matrix microstructural features and the shape, size, distribution and fraction of M-A constituents, the
154 microstructure of the HAZ is evaluated and discussed in detail below. The microstructural changes in the HAZ, as a
155 result of cold wire addition, are attributed to changes in the actual heat introduced to the weldment and the cooling
156 rate in the CGHAZ, when cold wire is added to the TSAW process. The large error bars for the HAZ weld samples
157 at 243 K (-30°C) are most likely related to the ductile-to-brittle transition temperature (DBTT) for this steel, which
158 is close to 243 K (-30°C). This interpretation is consistent with Graham [37] who reported that the Charpy absorbed
159 energy data for ferritic steels commonly exhibits large scatter in the DBTT region. However, the results show a
160 consistent trend in CVN impact energy by cold wire addition at different testing temperatures.



161 Fig. 3- Charpy impact toughness of the HAZ for steel samples welded by TSAW (no cold wire) and CWTSAW
 162 (cold wire addition at 25.4 cm/min and 76.2 cm/min). (a), (b) and (c) represent Charpy results at room temperature
 163 (RT), 243 K (-30°C) and 228 K (-45°C), respectively.
 164

165 **B. Microhardness and Macrostructure**

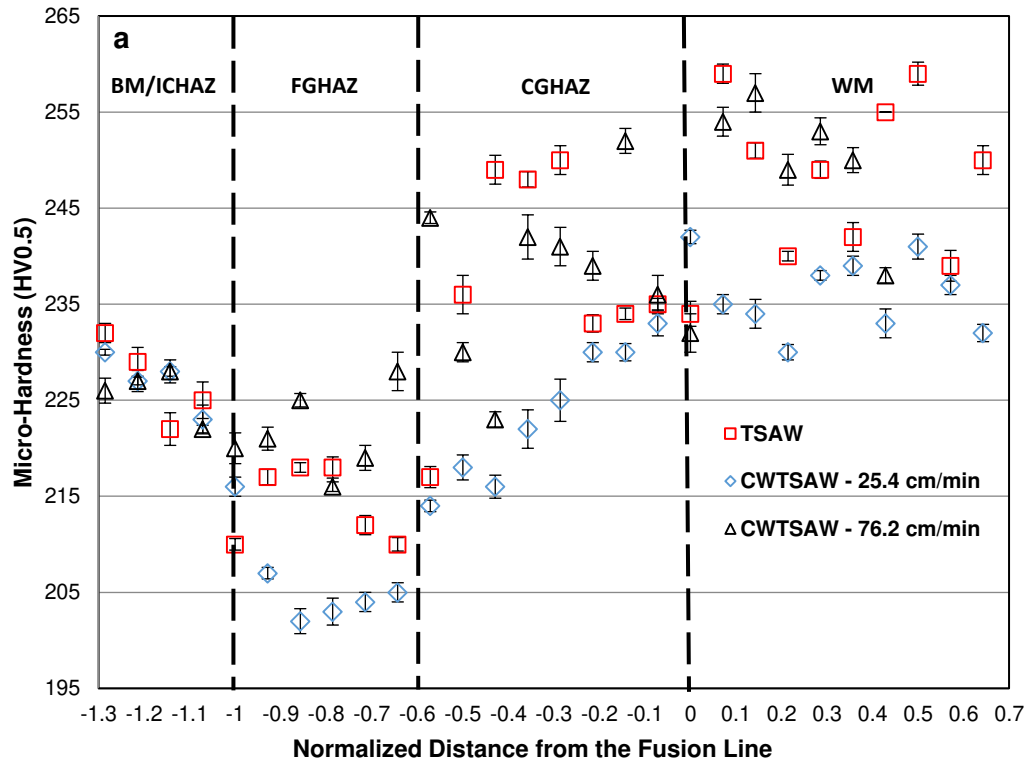
166 In addition to CVN testing, weld samples fabricated using the CWTSAW and TSAW processes were evaluated
 167 in terms of HAZ geometry and microhardness. The resultant CGHAZ area for the CWTSAW process was narrower
 168 than that for the TSAW process, due to lower actual heat introduced to the weldment by cold wire addition and the
 169 corresponding faster cooling rate. The reduction in the CGHAZ size was larger for the CW3 sample due to the
 170 higher cold wire feeding rate of 76.2 cm/min. Macrographs of three weld samples prepared via the CWTSAW and
 171 TSAW processes are shown in Figure 4. The results of four geometry measurements indicated a reduction in the
 172 CGHAZ area from $21.56 \pm 0.63 \text{ mm}^2$ for the TS weld to $20.30 \pm 0.50 \text{ mm}^2$ and $17.40 \pm 0.63 \text{ mm}^2$ for the CW1 and
 173 CW3 welds, respectively. The weld deposition rate was increased by 6% and 17% relative to the TSAW process,
 174 when the cold wire was fed at a rate of 25.4 cm/min (10 in/min) and 76.2 cm/min (30 in/min), respectively.



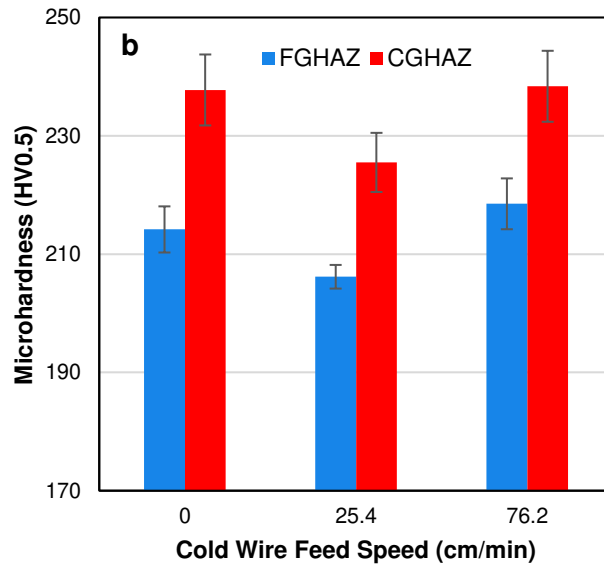
175
 176 Fig. 4- Macrographs of welded samples: (a) TS, (b) CW1 and (c) CW3.

177 Microhardness variations along the HAZ and the WM are depicted in Figure 5. The microhardness values of the
 178 as-received base metal (BM) was measured as $228 \pm 4 \text{ HV}$. As shown in Figure 5, the microhardness of the CGHAZ
 179 was reduced by the addition of a cold wire at 25.4 cm/min relative to the TSAW process. However, the average
 180 microhardness in the CGHAZ increased when the cold wire was fed at 76.2 cm/min. The different effects of cold
 181 wire addition on both microhardness and Charpy impact energy results is attributed to microstructural modifications
 182 taking place in the HAZ, due to changes in the actual welding heat input and consequent cooling rate, which are
 183 discussed later in this paper. The variation in the fraction, size, distribution and shape of M-A constituents (LBZ)

184 formed within the HAZ of microalloyed steel welds plays a significant role in the variation in mechanical properties
 185 in the HAZ, particularly the CGHAZ, which has also been confirmed by Bhadeshia [38,39].



186



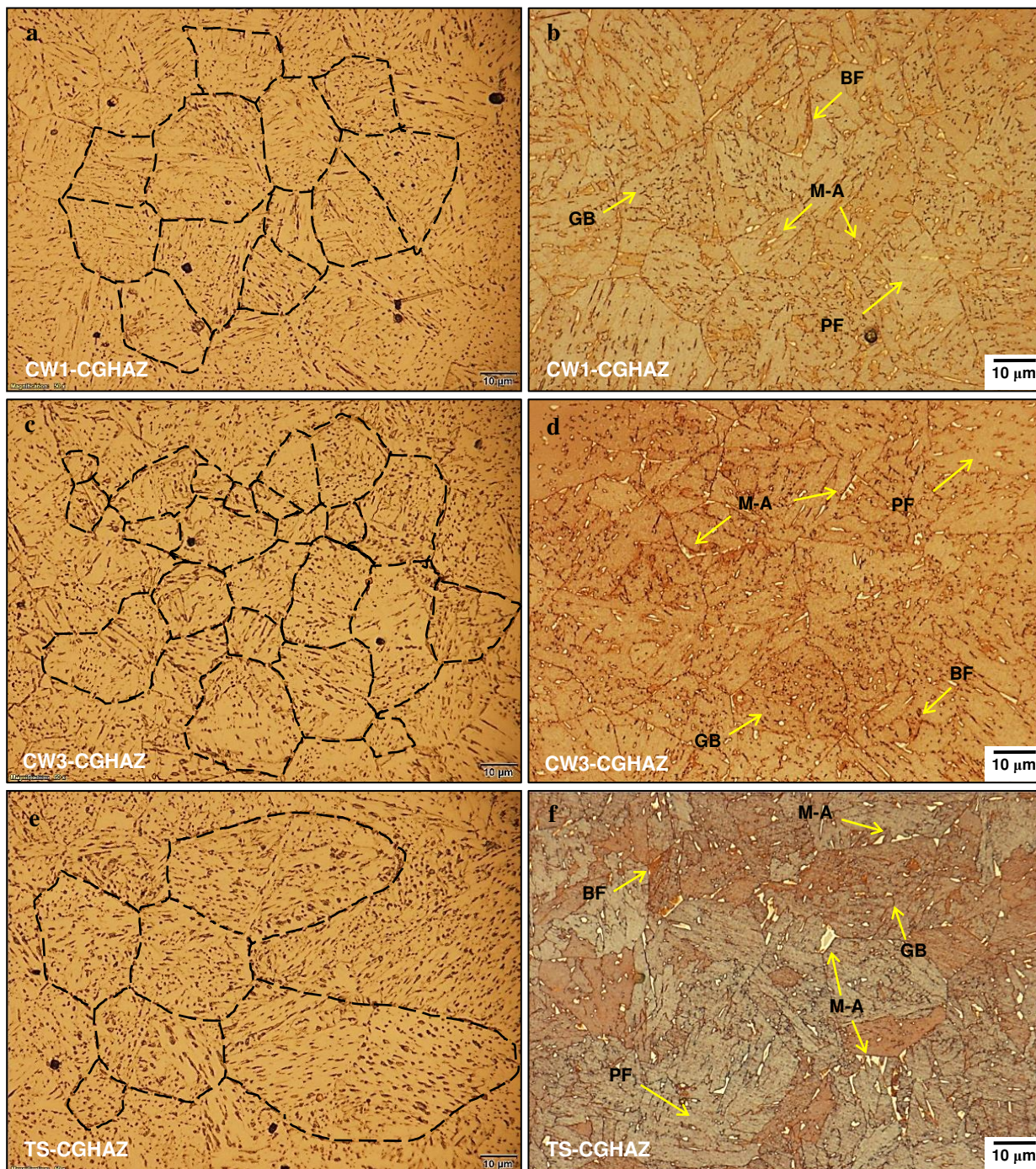
187 Fig. 5- (a) Microhardness variation within the weld samples. (b) Average microhardness, with standard deviation,
 188 for the FGHAZ and CGHAZ of steel samples welded by CWTSAW (cold wire addition at 25.4 cm/min and 76.2
 189 cm/min) and TSAW (no cold wire).
 190

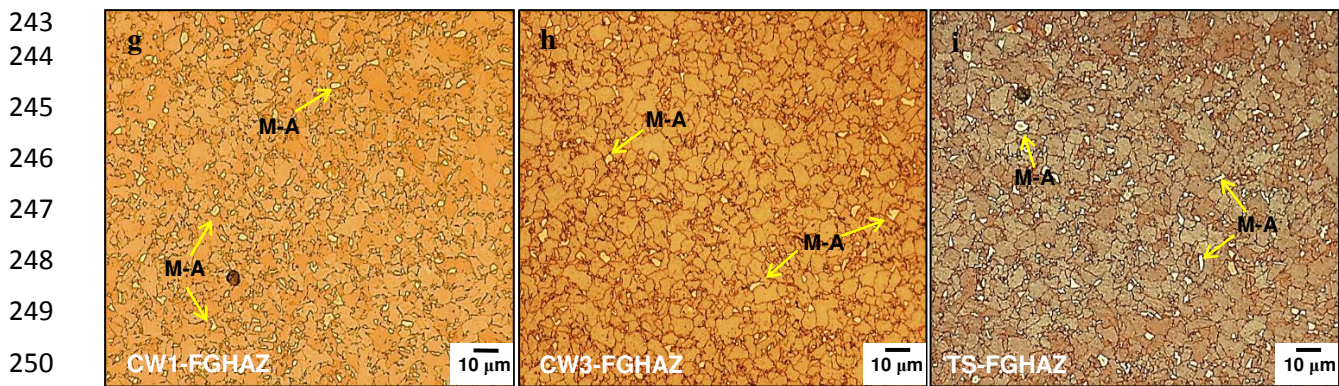
191 *C. Microstructure*

192 The microstructure of the X70 microalloyed steel consists of 87% polygonal ferrite, 9% granular bainite, 3%
 193 bainitic ferrite and a fine distribution of 1% M-A constituents with a PAG size of ~8 μm. The type and fraction of
 194 microstructural features along with the PAG formed in the region adjacent to the weld metal, i.e., the HAZ, are

195 altered due to the heat input and thermal cycles during welding. The PAG size in the CGHAZ (Figure 6(a)-(c)) and
 196 the FGHAZ decreased with the addition of the cold wire. The average PAG size in the CGHAZ (0-300 μm away
 197 from the fusion line) and FGHAZ (0-200 μm away from the CGHAZ/FGHAZ boundary) for the TS, CW1 and CW3
 198 weld samples are shown in Figure 7(a). The reduction in the PAG size in the CGHAZ is attributed to a reduction in
 199 the actual heat introduced to the weldment, a reduction in the retention time in the austenite temperature range, i.e.,
 200 1373-1673K (1100-1400°C), and an increase in the cooling rate by adding the cold wire. The M-A constituent, along
 201 with other microstructural features in the CGHAZ and FGHAZ of the three weld samples, are shown in Figure 6(d)-
 202 (i). The M-A constituents are revealed as white regions using modified LePera's etchant [34,35]. The amount of the
 203 microconstituents is shown in Figure 7(b). SEM secondary electron (SE) micrographs of the CGHAZ of the weld
 204 samples are depicted in Figure 8(a)-(c).

205
 206
 207
 208
 209
 210
 211
 212
 213
 214
 215
 216
 217
 218
 219
 220
 221
 222
 223
 224
 225
 226
 227
 228
 229
 230
 231
 232
 233
 234
 235
 236
 237
 238
 239
 240
 241
 242

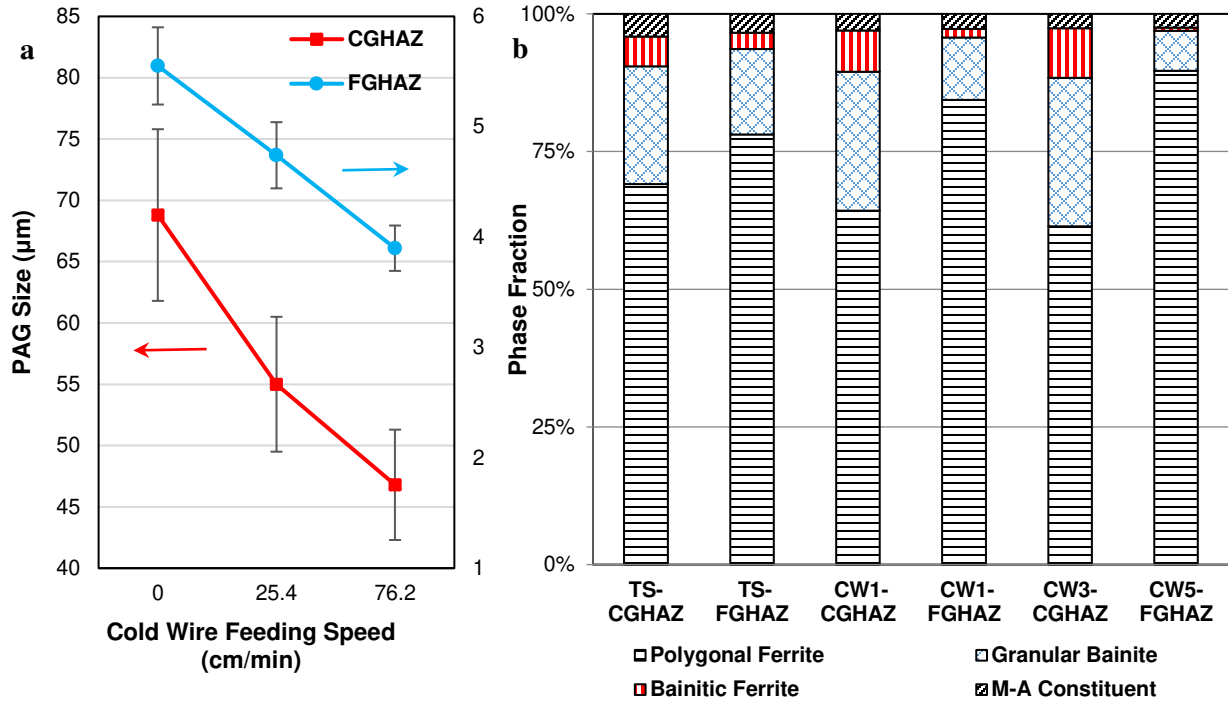




251 Fig. 6- Optical micrographs of the CGHAZ and FGHAZ for the CW1 sample (a,b,g), the CW3 sample (c,d,h) and
252 the TS sample (e,f,i). Images (a-f) and (g-i) are from the CGHAZ and FGHAZ, respectively.

253 **IV. DISCUSSION**

254 The PAG size influences the phase transformation temperature and kinetics during cooling [40,41]. Ying-Qiao
255 et al. [8] and Shome [42] reported that the size of PAGs in the HAZ depends on the local thermal cycle and the
256 PAG size increases with increasing welding heat input. Refining the PAG size influences the transformation
257 products, particularly the M-A constituents within the HAZ, which affect the toughness [11,12,32]. However, there
258 has only been limited work done to correlate the PAG size and M-A constituents [11,12,32,43]. In addition,
259 Bhadeshia [38,39], Yan et al. [44] and Matsuda et al. [45] have suggested that, in addition to the PAG size,
260 cooling rate affects the morphology of the M-A constituents, which also affect the toughness of the welded steel.
261 Kim et al. [46] have reported that M-A islands are the main metallurgical factor, which contribute to local
262 embrittlement of microstructures of welded microalloyed steels. They also stated that the Charpy impact toughness
263 of the CGHAZ of high strength low-carbon steels is a function of the fraction, morphology, carbon content and
264 distribution of the M-A islands. The work done by Lan et al. [47] indicated that the relatively fast cooling rate in the
265 HAZ of a low carbon steel led to the formation of slender M-A constituents with higher carbon levels and
266 segregated silicon in the M-A islands, which resulted in an increase in the martensite hardness in the HAZ. As such,
267 there is a concurrent effect of PAG size and cooling rate on the characteristics of the transformation products, in
268 particular the M-A constituents, in the HAZ of microalloyed steel welds. Figure 6(a)-(i) depicts optical micrographs
269 of the HAZ, revealing the PAGs and M-A constituents. The CGHAZ microstructure for the TS sample (with higher
270 heat input) has large PAGs, polygonal ferrite (PF), granular bainite (GB), bainitic ferrite (BF) and a higher fraction
271 of large M-A constituents, which are mostly formed along the PAG boundaries. In contrast with the TS sample, the
272 CGHAZ microstructure of the CW1 sample is composed of finer PAGs, PF, GB and BF associated with fine,
273 uniformly distributed M-A constituents. Due to the faster cooling rate in the CGHAZ of the CW3 sample (with the
274 fastest cold wire addition and the lowest actual heat input) compared with the CW1 sample, smaller PAGs were
275 formed in the CGHAZ of CW3, resulting in a lower fraction of elongated M-A constituents. However, longer M-A
276 constituents are formed in the CGHAZ of the CW3 sample, which may be attributed to a greater reduction in the
277 actual heat introduced to the weldment and the relatively fast cooling rate as a result of fast cold wire addition of
278 76.2 cm/min. However, the results indicate that the addition of the cold wire at 25.4 cm/min produced a favorable
279 effect on the microstructure, which was beneficial to the toughness. The microstructure of the FGHAZ of the CW1
280 and CW3 samples is composed of PF and less GB and BF with smaller M-A constituents compared with that of the
281 TS sample. However, fewer changes in the characteristics of the M-A constituents in the FGHAZ were observed by
282 varying the cold wire addition. Phase fraction analysis of the transformation products in the CGHAZ and FGHAZ of
283 the welded samples is indicated in Figure 7(b).



284 Fig. 7- (a) PAG size in the CGHAZ and FGHAZ and (b) microstructural constituent analysis in the FGHAZ and
 285 CGHAZ of microalloyed steel welds prepared by the CWTSAW (CW1 and CW3) and TSAW (TS) processes.
 286

287 The M-A fraction in the CGHAZ, determined from the optical micrographs, was 4.1%, 3.0% and 2.7% for the
 288 TS, CW1 and CW3 samples, respectively, indicating a reduction in the fraction of M-A as a consequence of PAG
 289 size reduction [10,11] by cold wire addition. The M-A fractions in the CGHAZ of the TS, CW1 and CW3 samples,
 290 determined from the SEM micrographs, were 5.4%, 3.3% and 3.1%, respectively. These values are similar to those
 291 obtained using optical microscopy, which confirms the validity of M-A identification using optical images. The M-
 292 A fractions in the FGHAZ of the TS, CW1 and CW3 samples were 3.6%, 2.7% and 2.4%, respectively. Quantitative
 293 analysis of the M-A size distribution is shown in Figure 9. The sizes shown in Figure 9 are presented as an
 294 equivalent spherical diameter determined from the area of each microconstituent analyzed. As shown in Figure
 295 6(b,d,f), the CGHAZ microstructure, particularly for the CW3 and TS samples, consists of more elongated shaped
 296 M-A constituents compared with the CW1 sample. A size distribution analysis was performed to evaluate the
 297 approximate size distribution of M-A constituents in the CGHAZ of the weld samples. In addition, image analysis
 298 carried out manually indicates that the fraction of M-A constituents in the CGHAZ with sizes larger than 1.5 μm for
 299 TS, CW1 and CW3 samples is 3.5%, 1.2% and 2.1%, respectively.

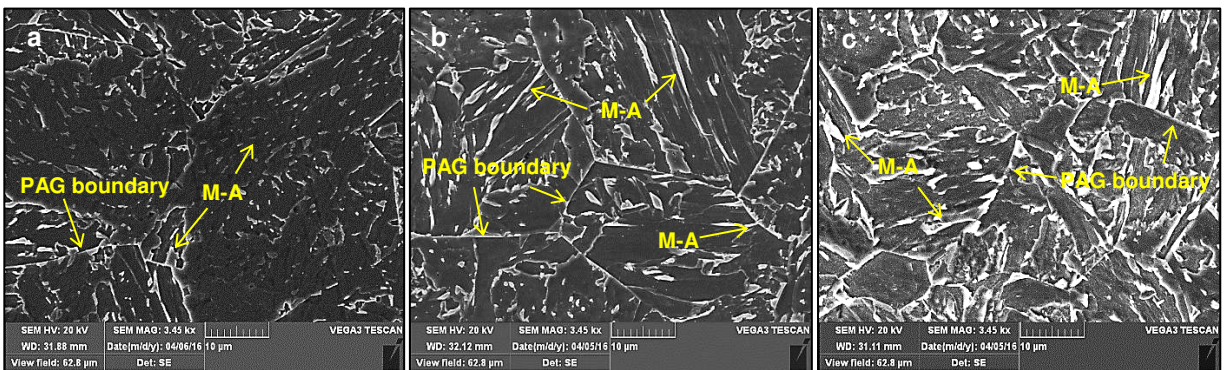
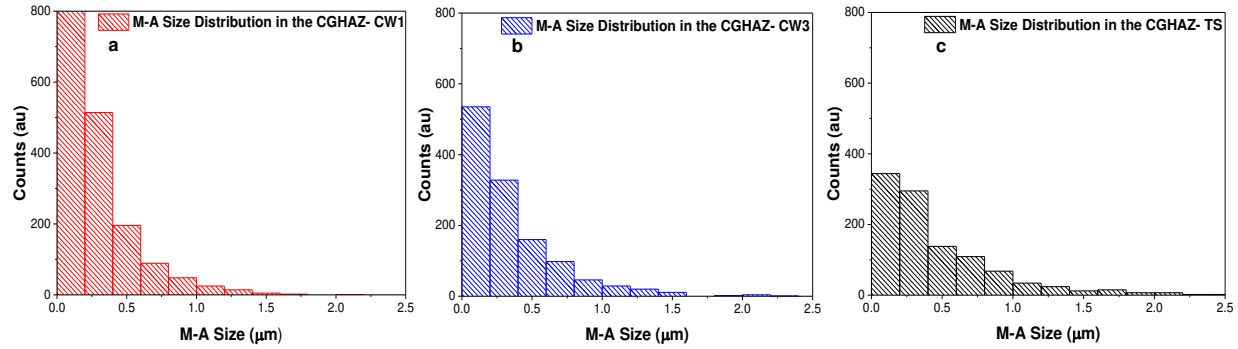


Fig. 8- SEM SE images of the CGHAZ for the (a) CW1, (b) CW3 and (c) TS samples.

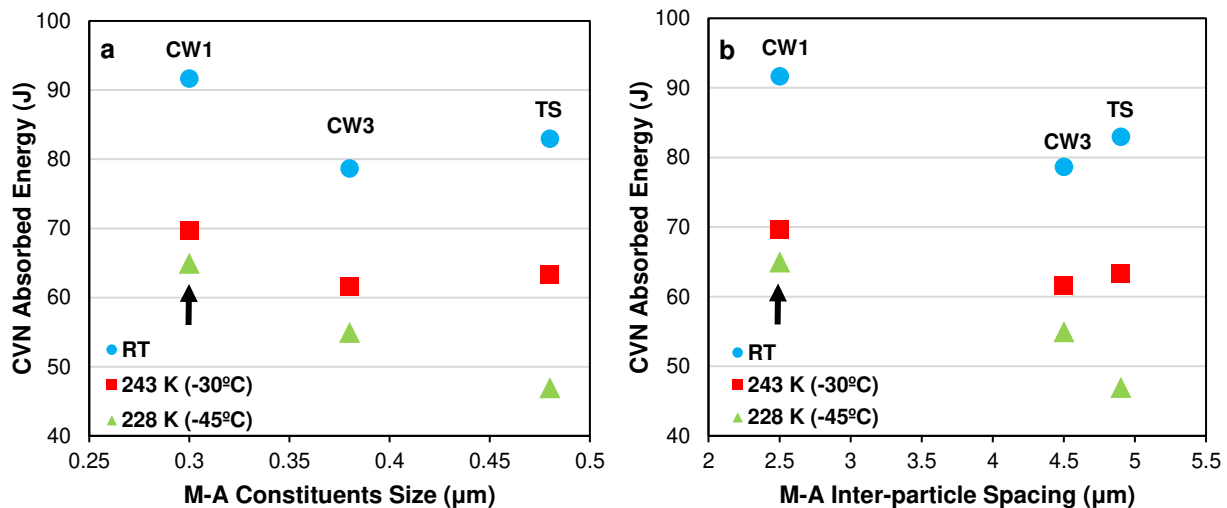


312
313 Fig. 9- Size distribution analysis of M-A constituent in the CGHAZ for the (a) CW1 (b) CW3 and (c) TS samples.

314 The fracture toughness of the CGHAZ of welded microalloyed steels is highly influenced by the shape, size,
315 distribution and fraction of M-A constituents in the CGHAZ [10,11,46]. The distribution of M-A constituents in the
316 CGHAZ of the weld samples was analyzed using the mean inter-particle spacing equation developed by Somekawa
317 et al. [48]. The equation takes into account the relative volume fraction, mean particle size and mean inter-particle
318 spacing.

319
$$\lambda_p = \frac{\pi d_p^2}{2\sqrt{3}f_p} - \frac{\sqrt{2}d_p}{\sqrt{3}} \quad [3]$$

320 where, λ_p , d_p and f_p are the mean inter-particle spacing, the mean particle size and the volume fraction, respectively.
321 To calculate the inter-particle spacing of M-A constituents in the CGHAZ, the measured M-A constituent volume
322 fraction along with the mean M-A sizes of 0.48 μm , 0.3 μm and 0.38 μm for the TS, CW1 and CW3 welds,
323 respectively, were used. The calculated mean M-A constituent spacings in the CGHAZ of the TS, CW1 and CW3
324 welds were 4.9 μm , 2.5 μm and 4.5 μm , respectively. Figure 10(a,b) indicates the variation in the Charpy impact
325 toughness in the HAZ as a function of M-A size and inter-particle spacing. As the M-A size and inter-particle
326 spacing decrease in the CGHAZ of the CW1 sample, the fracture toughness increases. Accordingly, the formation of
327 finely distributed M-A constituents in the CGHAZ of CW1 resulted in a beneficial effect on the fracture toughness.



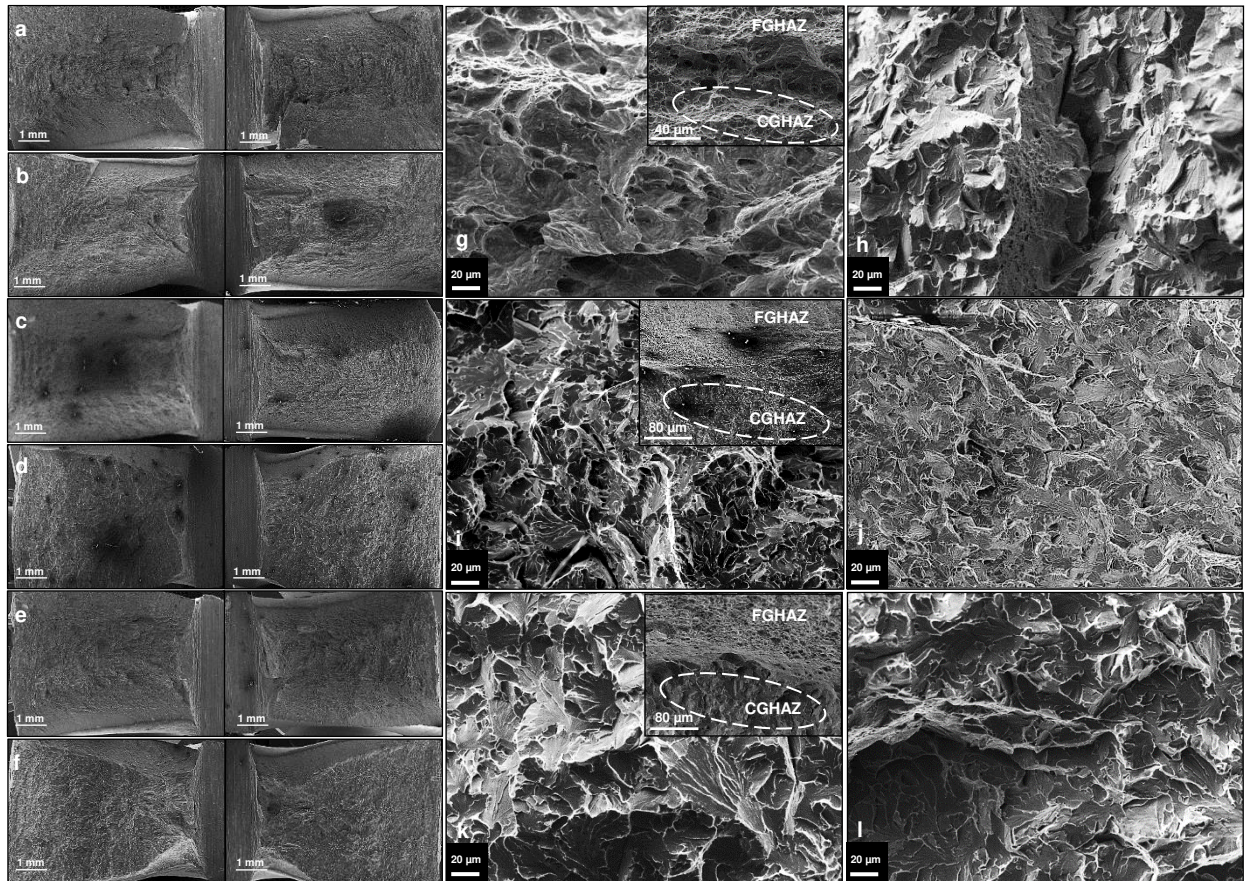
328
329 Fig. 10- Variation in the Charpy impact toughness as a function of (a) size and (b) inter-particle spacing of the M-A
330 constituents in the CGHAZ of the CW1, CW3 and TS samples.

331

332 The larger M-A constituents in the CGHAZ of the TS sample are due to the higher martensite start temperature
333 (Ms) for samples with larger PAGs [10,18,19,38]. Bhadeshia et al. [18,38], Heinze et al. [49] and Guimaraes [50]
334 suggested that a decrease in Ms temperature corresponds to a decrease in the PAG size, which results in a lower
335 volume fraction of martensite. According to the classical Koistinen-Marburger (KM) equation [51] and the
336 geometrical partitioning model by Fisher et al. [52], the fraction of martensite is a function of the amount of
337 undercooling below the Ms temperature. Based on the proposed model by Fisher et al. [52], the martensite volume
338 fraction formed in the early stages of the transformation is proportional to the PAG size cubed; hence, “the fraction
339 of the transformation needed to detect Ms is reached at a smaller undercooling when the PAG size is larger” [18].
340 Therefore, a coarser PAG size increases the fraction and size of the M-A constituent. Yu et al. [10] and Li et
341 al. [11] showed that a coarse PAG size, associated with a coarse M-A constituent, is the dominant factor in
342 promoting brittle fracture in the CGHAZ. Accordingly, there is a concurrent effect of both grain size refinement and
343 M-A transformation, which plays a significant role in the strength and toughness of the HAZ. Due to the formation
344 of the M-A constituent, there is a higher proportion of LBZs in the CGHAZ of the TS sample compared with the
345 CW1 and CW3 samples. This shows up as higher microhardness values in the CGHAZ for the TS sample relative to
346 the CW1 and CW3 samples. Also, a narrower distribution of fine M-A constituents (LBZs) inside the ferritic matrix in
347 the CGHAZ of the CW1 sample resulted in a higher fracture toughness for the HAZ at the various testing
348 temperatures. However, coarser PAGs with large M-A constituents, which are mostly formed along the PAG
349 boundaries, lead to inferior toughness properties in the HAZ of the TS sample. This inferior toughness, due to the
350 formation of M-A constituents along PAG boundaries, has been confirmed by the research work done by Davis et
351 al. [13,14] and Reichert et al. [15]. They found that the combination of an elongated shape and the formation of a
352 network of M-A constituents along the PAG boundaries is most detrimental to fracture properties. With reference to
353 the CW3 sample, Yan et al. [44] and Bhadeshia [38,39] have proposed that, in addition to the PAG size, the shape,
354 size and distribution of the M-A constituents along with the martensite carbon content are influenced by the cooling
355 rate in the HAZ, which affects toughness of welded microalloyed steels [53]. Elongated M-A constituents, with
356 large inter-particle spacing, are formed in the CGHAZ of the CW3 sample due to the relatively faster cooling rate in
357 the CGHAZ as a result of fast cold wire addition relative to the CW1 sample. This leads to a slight decrease in
358 toughness for the HAZ of the CW3 sample compared with the CW1 sample (Figure 10). This phenomenon has also
359 been confirmed by the work done by Davis et al. [13], Kim et al. [46] and Lan et al. [47], who have suggested that
360 the morphology of martensite changes and the carbon content of martensite increases in the M-A constituents as the
361 cooling rate in the CGHAZ increases. As such, the relatively faster cooling rate in the CGHAZ of the CW3 sample
362 compared with the CW1 sample led to the formation of elongated M-A constituents with larger inter-particle
363 spacing and higher carbon levels and segregated silicon to the M-A islands.

364
365
366
367
368
369
370
371
372
373
374
375
376
377
378
379
380

381
382
383
384
385
386
387
388
389
390
391
392
393
394
395
396
397
398
399
400
401
402
403
404
405



406
407
408
409

Fig. 11- SEM SE fractographs for the (a,b) CW1, (c,d) CW3 and (e,f) TS specimens. SEM SE micrographs showing the fracture surfaces in the CGHAZ for the (g,h) CW1, (i,j) CW3 and (k,l) TS specimens. The insets in (g), (i) and (k) show the boundary between the FGHAZ and CGHAZ in the weld specimens. Micrographs (a,c,e,g,i,k) and (b,d,f,h,j,l) are from Charpy samples tested at RT and 243 K (-30°C), respectively.

410
411
412
413
414
415
416
417
418
419
420
421
422
423
424
425
426
427
428

According to the impact toughness results shown in Figure 10, the toughness of the HAZ of the TS sample was lower compared with that of the CW1 sample, which is attributed to the formation of a high fraction of elongated and widely spaced M-A constituents inside and along the PAG boundaries as a result of the higher actual heat input. Lowering the actual heat introduced to the weldment, by addition of the cold wire at 25.4 cm/min, altered the size, shape, distribution and fraction of the M-A constituent, leading to an improvement in the HAZ toughness of the CW1 sample. The reduction in toughness by increasing welding heat input has been confirmed in the literature [16,42,54]. However, when the cold wire was fed at a faster rate of 76.2 cm/min, the HAZ toughness was diminished due to the formation of large, widely spaced elongated M-A constituents inside and along PAG boundaries as a result of the faster cooling rate. The influence of the fast cooling rate on the fracture toughness of the HAZ of microalloyed steels has been well documented previously through the work done by Hutchinson et al. [55], Yan et al. [44] and Bhadeshia [38,39]. A faster cooling rate provides a greater driving force for martensite transformation, which increases the fraction of martensite within the M-A constituents in the CGHAZ [47]. The faster cooling rate also influences the morphology of the M-A constituents, leading to more elongated shapes and detrimental effects on fracture toughness [38,44,55]. Cracks, initiated at large elongated M-A constituents, can connect and form a long continuous long crack, resulting in brittle cleavage fracture. A low fraction of finely distributed fine M-A constituents can act as crack arrestors for secondary cracks, which is beneficial to toughness [56]. In addition, it is generally accepted that the formation of large slender shaped M-A constituents in the CGHAZ of welded microalloyed steels is detrimental to the HAZ fracture toughness. However, regardless of the shape and size of M-A constituents, spacing of the hard phases in the soft matrix (i.e., ferritic matrix in the CGHAZ

429 of the welded microalloyed steel) influences the propagation of the cracks in a manner similar to composite
430 materials. As the spacing between hard particles (or phases) decreases, the crack will face a hard phase at a shorter
431 distance, which stops the crack or makes it harder for the crack to propagate. In addition, slender shaped hard phases
432 (or particles) promote the propagation of any cracks due to the higher stress concentration at the tip of the sharp
433 particles.

434 The fracture surface morphologies of the HAZ at RT and 243 K (-30°C) for the CW1, CW3 and TS Charpy
435 samples are illustrated in Figure 11(a,b,g,h), 11(c,d,i,j) and 11(e,f,k,l), respectively. The boundary between the
436 CGHAZ and FGHAZ on the fracture surface is shown in the inset micrographs in Figure 11(g,i,k). The fracture
437 surface for the FGHAZ and CGHAZ of the CW1 weld sample at RT is fully ductile and the fracture mechanism
438 involves microvoid coalescence (MVC). However, the fracture mechanism in the FGHAZ and CGHAZ for both the
439 CW3 and TS samples at RT is different, i.e., MVC and quasi-cleavage, respectively, resulting in ductile and quasi-
440 brittle fracture in the FGHAZ and CGHAZ at RT. Due to the large PAG size in the CGHAZ of the TS sample, large
441 cleavage facets are present on the fracture surface. Moreover, the formation of large, elongated and widely spaced
442 M-A constituents in the CGHAZ of the CW3 and TS samples contributed to lowering of the Charpy energy in the
443 HAZ. A combination of MVC and quasi-cleavage fracture is seen on the CGHAZ fracture surface of the CW1
444 sample tested at 243 K (-30°C). However, the CGHAZ fracture surface of the TS sample consists of a mixture of
445 cleavage and intergranular facets, resulting in brittle fracture in the CGHAZ of the TS sample tested at 243 K (-
446 30°C) [57]. Similar to the TS sample, intergranular fracture along with cleavage is the dominant fracture
447 mechanism of the CGHAZ of the CW3 sample, due to the formation of the elongated M-A constituents along the
448 PAGs with large inter-particle spacing. Finer cleavage facets are evident on the CGHAZ fracture surface of the
449 CW3 sample because of the formation of a finer PAG size in the CGHAZ of the CW3 sample due to the faster
450 cooling rate (lower actual heat input by faster cold wire addition) in the CGHAZ compared with the other two weld
451 samples.

452 The fracture mechanism at 228 K (-45°C) in the FGHAZ of the three weld samples was MVC, however,
453 cleavage and intergranular fracture were observed to be the dominant mechanism in the CGHAZ of the weld
454 samples. Since, the fracture mechanism of the three weld samples at 228 K (-45°C) was similar to the fracture
455 mechanism for the CW3 and TS samples at 243 K (-30°C), the fractographs at 228 K (-45°C) are not shown here.
456 The M-A constituent is significantly harder than the internal grain microstructure, so that cracks initiate easily along
457 large M-A constituents. Aucott et al. [58] have suggested that the toughness of a welded X65 linepipe steel was
458 reduced by formation of coarse size particles with large inter-particle spacing. Moeinifar et al. [1] concluded from
459 their microstructural study on multiple-wire TSAW samples that the size and shape of M-A constituents are
460 significant factors affecting the Charpy impact properties of the CGHAZ and that microcrack nucleation may occur
461 from M-A islands at the intersection of PAG boundaries. Moreover, Li et al. [56] found that an intercritically
462 reheated CGHAZ demonstrated the lowest toughness, due to the presence of M-A constituents with high carbon
463 content martensite. The large elongated shaped M-A constituents with large inter-particle spacing in the CGHAZ of
464 the CW3 and TS samples of this work formed mostly along the PAG boundaries and can promote the formation of
465 microcracks, resulting in brittle/quasi-brittle fracture in the HAZ.

466 V. CONCLUSIONS

467 The influence of the cold wire addition rate, in the recently developed cold wire tandem submerged arc welding
468 (CWTSAW) process, on the microstructural characteristics and mechanical properties of the HAZ of a welded
469 microalloyed steel has been studied for the first time. Cold wire addition resulted in a reduction in the prior austenite
470 grain (PAG) size in the coarse grained heat affected zone (CGHAZ). Microstructural analysis indicated that the
471 fraction of martensite-austenite (M-A) constituents in the CGHAZ was reduced and the distribution, size and shape
472 were altered, when a cold wire was added to the TSAW process. The cold wire addition at 25.4 cm/min showed a
473 reduction in the fraction of M-A constituents along with a uniform distribution of finer M-A constituents in the
474 ferritic matrix due to a reduction in the actual welding heat input and the PAG size, which resulted in an
475 improvement in fracture toughness of the HAZ. The changes to the fraction and characteristics of the M-A

476 constituents in the HAZ of the cold wire sample (25.4 cm/min) relative to the sample with no cold wire are
477 attributed to the lower actual heat introduced to the weldment and the resulting faster cooling rate, lower peak
478 temperature and the formation of finer PAGs by cold wire addition. Although the PAG size was further reduced
479 when the cold wire was fed at 76.2 cm/min (compared with the cold wire (25.4 cm/min) and TSAW weld samples),
480 due to a faster cooling rate in the CGHAZ of the 76.2 cm/min cold wire sample, elongated shaped M-A constituents
481 were formed. The relatively large elongated M-A constituents with large inter-particle spacing, which mostly
482 formed along the PAG boundaries in the CGHAZ, of the TSAW and cold wire (76.2 cm/min) samples compared
483 with those of the cold wire sample (25.4 cm/min) led to inferior toughness properties in the HAZ of the former
484 samples, since the larger M-A constituents can stimulate the formation of microcracks leading to intergranular
485 fracture.

486 ACKNOWLEDGMENTS

487 The authors would like to thank the Natural Sciences and Engineering Research Council (NSERC) of Canada,
488 Evraz Inc. NA, TransCanada PipeLines Ltd., Enbridge Pipelines Inc., UT quality Inc. and Alliance Pipeline Ltd for
489 financial support. Special thanks go to the Research and Development Division of Evraz Inc. NA for providing
490 equipment and technical assistance to conduct the welding runs and Charpy testing.

491 REFERENCES

- 492 [1] S. Moeinifar, A. H. Kokabi, and H. R. Madaah Hosseini: *J. Mater. Process. Technol.*, 2011, vol. 211, pp. 368–75.
493 [2] D. V. Kiran, S.A. Alam, and A. De: *J. Mater. Eng. Perform.*, 2013, vol. 22, pp. 988–94.
494 [3] ESAB: *Submerged Arc Welding (Technical Handbook)*, TX, 2013.
495 [4] D.M. Viano, N.U. Ahmed, G.O. Schumann, D.M. Viano, N.U. Ahmed, and G.O. Schumann: *Sci. Technol. Weld. Join.*,
496 2000, vol. 5, pp. 26–34.
497 [5] Y. Watanabe, K. Yoshii, and Y. Yoshida: *Development of 590N/mm² Steel with Good Weldability for Building*
498 *Structures, Technical Report No. 90*, 2004.
499 [6] D.W. Nugent, R.M., Dybas, R.J., Hunt, J.F., Meyer: *Submerged Arc Welding. AWS Welding Handbook*, 8th Ed.,
500 American Welding Society, Miami, 2009.
501 [7] S. Shen, I.N.A. Oguocha, and S. Yannacopoulos: *J. Mater. Process. Technol.*, 2012, vol. 212, pp. 286–94.
502 [8] Ying Qiao Zhang, Han Qian Zhang, Jin Fu Li, and Wei Ming Liu: *J. Iron Steel Res. Int.*, 2009, vol. 16, pp. 73–80.
503 [9] Z.H. Xia, X.L. Wan, X.L. Tao, and K.M. Wu: *Adv. Mater. Res.*, 2012, vol. 538–541, pp. 2003–8.
504 [10] L. Yu, H.H. Wang, T.P. Hou, X.L. Wang, X.L. Wan, and K.M. Wu: *Sci. Technol. Weld. Join.*, 2014, vol. 19, pp. 708–
505 14.
506 [11] X. Li, X. Ma, S.V. Subramanian, Ch. Shang, and R.D.K. Misra: *Mater. Sci. Eng. A*, 2014, vol. 616, pp. 141–47.
507 [12] X. Li, Y. Fan, X. Ma, S.V. Subramanian, and Ch. Shang: *Mater. Des.*, 2015, vol. 67, pp. 457–63.
508 [13] C.L. Davis and J.E. King: *Mater. Sci. Technol.*, 1993, vol. 9, pp. 8–15.
509 [14] C.L. Davis and J.E. King: *Metall. Mater. Trans. A*, 1994, vol. 25, pp. 563–73.
510 [15] J.M. Reichert, T. Garcin, M. Militzer, and W.J. Poole: in *9th Int. Pipeline Conf.*, American Society of Mechanical
511 Engineering, Calgary, AB, 2014.
512 [16] S. Moeinifar, A.H. Kokabi, and H.R. Madaah Hosseini: *Mater. Des.*, 2010, vol. 31, pp. 2948–55.
513 [17] E. Gharibshahiyan, A. Honarbakhsh, N. Parvin, and M. Rahimian: *Mater. Des.*, 2011, vol. 32, pp. 2042–48.
514 [18] H.S. Yang and H.K.D.H. Bhadeshia: *Scr. Mater.*, 2009, vol. 60, pp. 493–95.
515 [19] A. Garcia-Junceda, C. Capdevila, F.G. Caballero, C. Garcia, and D. Andre: *Scr. Mater.*, 2008, vol. 58, pp. 134–37.
516 [20] M.F. Mruczek and P.J. Konkol: *Cold Wire Feed Submerged Arc Welding: Technical Report*, Advanced Technology
517 Institute (ATI), Johnstown, PA, 2006.
518 [21] M. Ramakrishnan and V. Muthupandi: *Int. J. Adv. Manuf. Technol.*, 2012, pp. 1–12.
519 [22] M. Ramakrishnan, K. Padmanaban, and V. Muthupandi: *Int. J. Adv. Manuf. Technol.*, 2013, vol. 68, pp. 293–316.
520 [23] M. Mohammadjoo, S. Kenny, J.B. Wiskel, D.G. Ivey, and H. Henein: in *54th Annual Conf. Metall.*, Canadian Institute
521 of Mining, Metallurgy and Petroleum, Toronto, ON, 2015, pp. 1–13.
522 [24] M. Mohammadjoo, S. Kenny, L. Collins, H. Henein, and D.G. Ivey: *Int. J. Adv. Manuf. Technol.*, 2016, doi:
523 10.1007/s00170-016-8910-z, pp. 1–15.
524 [25] N. Shikanai, S. Mitao, and S. Endo: *Recent Development in Microstructural Control Technologies through the Thermo-*
525 *Mechanical Control Process (TMCP) with JFE Steel's High-Performance: JFE Technical Report No. 18 Plates*, JFE
526 Steel, Tokyo, 2007.
527 [26] K.E. Easterling: *Introduction to the Physical Metallurgy of Welding*, Butterworth-Heinemann Ltd, Oxford, 1992.
528 [27] B. De Meester: *ISIJ Int.*, 1997, vol. 37, pp. 537–51.
529 [28] L.P. Connor and R.L. O'Brien: *Welding Handbook: Welding Technology*, American Welding Society, Miami, 1987.

- 530 [29] ASTM: *ASTM E23-12C: Standard Test Methods for Notched Bar Impact Testing of Metallic Materials*, ASTM
531 International, PA, 2012.
- 532 [30] ASTM: *E384: Standard Test Method for Knoop and Vickers Hardness of Materials*, ASTM International, PA, 2012.
- 533 [31] ASTM: *E3-11: Standard Guide for Preparation of Metallographic Specimens*, ASTM International, PA, 2011.
- 534 [32] Y. Prawoto, N. Jasmawati, and K. Sumeru: *J. Mater. Sci. Technol.*, 2012, vol. 28, pp. 461–66.
- 535 [33] ASTM: *E112-12: Standard Test Methods for Determining Average Grain Size*, ASTM International, PA, 2012.
- 536 [34] F.S. LePera: *Metallography*, 1979, vol. 12, pp. 263–68.
- 537 [35] M. Mohammadijoo, H. Henein, and D.G. Ivey: in *Microsc. Soc. Canada 43rd Annu. Meet.*, Edmonton, AB, 2016,
538 pp. 68–69.
- 539 [36] ASTM: *ASTM E562-11: Standard Test Method for Determining Volume Fraction by Systematic Manual Point Count*,
540 ASTM International, PA, 2011.
- 541 [37] S.M. Graham: *J. Test. Eval.*, 2005, vol. 33.
- 542 [38] H.K.D.H. Bhadeshia: in *Int. Semin. Weld. High Strength Pipeline Steels*, CBMM and The Minerals, Metals and
543 Materials Society, The Minerals, Metals and Materials Society (TMS), USA, 2013, pp. 99–106.
- 544 [39] H.K.D.H. Bhadeshia: *Mater. Sci. Forum*, 2014, vol. 783–786, pp. 2129–35.
- 545 [40] M. Shome, O.P. Gupta, and O.N. Mohanty: *Metall. Mater. Trans. A*, 2004, vol. 35A, pp. 985–96.
- 546 [41] G. Spanos, R.W. Fonda, R.A. Vandermeer, and A. Matuszeski: *Metall. Mater. Trans. A*, 1995, vol. 26A, pp. 3277–93.
- 547 [42] M. Shome: *Mater. Sci. Eng. A*, 2007, vol. 445–446, pp. 454–60.
- 548 [43] R. Cao, J. Li, D.S. Liu, J.Y. Ma, and J.H. Chen: *Metall. Mater. Trans. A*, 2015, vol. 46A, pp. 2999–3014.
- 549 [44] P. Yan and H.K.D.H. Bhadeshia: *Mater. Sci. Technol.*, 2015, vol. 31, pp. 1066–76.
- 550 [45] F. Matsuda, K. Ikeuchi, Y. Fukada, Y. Horii, H. Okada, T. Shiwaku, C. Shiga, and S. Suzuki: *Transactions JWRI*, 1995,
551 vol. 24, pp. 1–24.
- 552 [46] B.C. Kim, S. Lee, N.J. Kim, and D.Y. Lee: *Metall. Mater. Trans. A*, 1991, vol. 22, pp. 139–49.
- 553 [47] L. Lan, Ch. Qiu, and D. Zhao: *J. Mater. Sci.*, 2012, vol. 47, pp. 4732–42.
- 554 [48] H. Somekawa and T. Mukai: *Mater. Trans.*, 2006, vol. 47, pp. 995–98.
- 555 [49] C. Heinze, A. Pittner, M. Rethmeier, and S.S. Babu: *Comput. Mater. Sci.*, 2013, vol. 69, pp. 251–60.
- 556 [50] J.R.C. Guimaraes and P.R. Rios: *J. Mater. Sci.*, 2010, vol. 45, pp. 1074–77.
- 557 [51] D.P. Koistinen and R.E. Marburger: *Acta Metall.*, 1959, vol. 7, pp. 59–60.
- 558 [52] J.C. Fisher, J.H. Hollomon, and D. Turnbull: *Trans. Am. Inst. Min. Metall. Eng.*, 1949, vol. 185, pp. 691–700.
- 559 [53] C.R. Brooks: *Principles of the Heat Treatment of Plain Carbon and Low-Alloy Steel*, ASM International, Ohio, 1996.
- 560 [54] G.-L. Liang, S.-W. Yang, and H.-B. Wu: *Rare Met.*, 2013, vol. 32, pp. 129–33.
- 561 [55] B. Hutchinson, J. Komenda, G.S. Rohrer, and H. Beladi: *Acta Mater.*, 2015, vol. 97, pp. 380–91.
- 562 [56] Y. Li and T.N. Baker: *Mater. Sci. Technol.*, 2010, vol. 26, pp. 1029–40.
- 563 [57] M. Shome, O.P. Gupta, and O.N. Mohanty: *Metall. Mater. Trans. A*, 2004, vol. 35A, pp. 985–96.
- 564 [58] L. Aucott, S.W. Wen, and H. Dong: *Mater. Sci. Eng. A*, 2015, vol. 622, pp. 194–203.
- 565

566

Figure Captions:

567 Fig. 1- CWTSAW process setup. (a) Schematic view of joint configuration along with the positioning of the
568 electrodes and cold wire and (b) welding setup designed at Evraz Inc. NA.

569 Fig. 2- (a) Schematic view of the CVN specimen extraction from the weld sample. (b) Microhardness mapping
570 along the BM, HAZ and WM of a typical weld prepared by CWTSAW. The micrograph in the inset shows an
571 indentation in the CGHAZ.

572 Fig. 3- Charpy impact toughness of the HAZ for steel samples welded by TSAW (no cold wire) and CWTSAW
573 (cold wire addition at 25.4 cm/min and 76.2 cm/min). (a), (b) and (c) represent Charpy results at room temperature
574 (RT), 243 K (-30°C) and 228 K (-45°C), respectively.

575 Fig. 4- Macrographs of welded samples: (a) TS, (b) CW1 and (c) CW3.

576 Fig. 5- (a) Microhardness variation within the weld samples. (b) Average microhardness, with the standard
577 deviation, for the FGHAZ and CGHAZ of steel samples welded by the CWTSAW (cold wire addition at 25.4
578 cm/min and 76.2 cm/min) and TSAW (no cold wire).

579 Fig. 6- Optical micrographs of the CGHAZ and FGHAZ for the CW1 sample (a,b,g), the CW3 sample (c,d,h) and
580 the TS sample (e,f,i). Images (a-f) and (g-i) are from the CGHAZ and FGHAZ, respectively.

581 Fig. 7- (a) PAG size in the CGHAZ and FGHAZ and (b) microstructural constituent analysis in the FGHAZ and
582 CGHAZ for microalloyed steels welded by the CWTSAW (CW1 and CW3) and TSAW (TS) processes.

583 Fig. 8- SEM SE images of the CGHAZ for the (a) CW1, (b) CW3 and (c) TS samples.

584 Fig. 9- Size distribution analysis of M-A constituent in the CGHAZ for the (a) CW1 (b) CW3 and (c) TS samples.

585 Fig. 10- Variation in the Charpy impact toughness as a function of (a) size and (b) inter-particle spacing of the M-A
586 constituents in the CGHAZ of the CW1, CW3 and TS samples.

587 Fig. 11- SEM SE fractographs for the (a,b) CW1, (c,d) CW3 and (e,f) TS specimens. SEM SE micrographs showing
588 the fracture surfaces in the CGHAZ for the (g,h) CW1, (i,j) CW3 and (k,l) TS specimens. The insets in (g), (i) and
589 (k) show the boundary between the FGHAZ and CGHAZ in the weld specimens. Micrographs (a,c,e,g,i,k) and
590 (b,d,f,h,j,l) are from Charpy samples tested at RT and 243 K (-30°C), respectively.

591
592
593
594
595
596
597
598
599

Tables:

Table I. X70 microalloyed steel and electrode compositions (wt%)

X70 composition										
C	P	S	Mn	Si	N	V+Mo+Nb+Ti	Cu+Ni+Cr+Sn+Al+Ca		Pcm	
0.04	0.01	0.001	1.76	0.24	0.0098	0.21	0.60		0.175	
Electrode and cold-wire composition										
Symbol	C	P	S	Mn	Si	Mo	Ni	Cr	Cu	
BA-S2Mo	0.10	0.007	0.01	1.04	0.1	0.56	0.02	0.03	0.03	

Table II. Welding process parameters

Process Parameter	Unit	Value		
Current- Lead Electrode	A	1040		
Current- Trail Electrode	A	830		
Voltage- Lead Electrode	V	30		
Voltage- Trail Electrode	V	34		
Feed Speed- Lead Electrode	cm/min (in/min)	254 (100)		
Feed Speed- Trail Electrode	cm/min (in/min)	203 (80)		
Welding Travel Speed	cm/min (in/min)	160 (63)		
		CW1	CW3	TS
Cold Wire Position	--	Lagging	Lagging	NA
Cold Wire Angle	degree	63	63	NA
Cold Wire Feed Speed	cm/min (in/min)	25.4 (10)	76.2 (30)	NA